https://doi.org/10.5194/egusphere-2025-243
Preprint. Discussion started: 6 February 2025

Fertilization-driven Pulses of Atmospheric Nitrogen Dioxide Complicate Air Pollution in Early Spring over North China

Tian Feng,[1] Guohui Li,[2,*] Shuyu Zhao,[3] Naifang Bei,[4] Xin Long,[5] Yuepeng Pan,[6] Yu Song,[7] Ruonan Wang,[2] Xuexi Tie,[2] Luisa T. Molina[8]

[1] Department of Geography & Spatial Information Techniques, Ningbo University, Ningbo, China
[2] KLACP, State Key Laboratory of Loess and Quaternary Geology, Institute of Earth Environment, Chinese Academy of Sciences, Xi'an, China
[3] Ningbo Meteorological Bureau, Ningbo, China
[4] School of Human Settlements and Civil Engineering, Xi'an Jiaotong University, Xi'an, China
[5] Research Center for Atmospheric Environment, Chongqing Institute of Green and Intelligent Technology, Chinese Academy of Sciences, Chongqing, China
[6] State Key Laboratory of Atmospheric Boundary Layer Physics and Atmospheric Chemistry (LAPC), Institute of Atmospheric Physics, Chinese Academy of Sciences, Beijing, China
[7] State Key Joint Laboratory of Environmental Simulation and Pollution Control, Department of Environmental Science, Peking University, Beijing, China
[8] Molina Center for Energy and the Environment, La Jolla, CA, USA

*Corresponding author. Email: ligh@ieecas.cn

https://doi.org/10.5194/egusphere-2025-243
Preprint. Discussion started: 6 February 2025

Abstract

Atmospheric NO_2 has shown periodic conspicuous pulses in tropospheric column in March over North China during the past two decades. However, these repetitive pulses have never been reported and its underlying causes remain unclear. Here, we present robust evidence to demonstrate that agricultural fertilization drives the early-spring NO_2 column increases. The fertilization-driven soil NO_X (=NO+NO_2) emissions, comparable to anthropogenic sources, exert complicated influences on regional air quality. They significantly reduce nocturnal and diurnal O_3 concentrations in agricultural areas in early spring, distinct from the scenarios in summer, but increase fine particulate matter ($PM_{2.5}$) concentrations *via* strongly enhancing nitrate aerosol formation. The impact also extends to urban areas, approximately half that of agricultural areas. These findings are with increasing implications for coordinated control of $PM_{2.5}$ and O_3 under global warming. We thus suggest that reducing NO_X emissions in croplands is essential to achieve better air quality in agricultural countries and regions.

Short Summary

Impacts of agricultural fertilization on nitrogen oxide and air quality are becoming more pronounced with continuous reductions in fossil fuel sources in China. We report that atmospheric nitrogen dioxide pulses driven by agricultural fertilizations largely complicate air pollution in North China, highlighting the necessity of agricultural emission control.

Keywords: Nitrogen Dioxide, Fertilization, Air Pollution, Ozone, $PM_{2.5}$

https://doi.org/10.5194/egusphere-2025-243
Preprint. Discussion started: 6 February 2025

1 Introduction

Nitrogen oxide (NO_X = NO + NO_2) is a major air pollutant in the troposphere and a key precursor to ozone (O_3) and fine particulate matter ($PM_{2.5}$) due to its photochemical properties (Seinfeld and Pandis, 2006; Zhang et al., 2015). It is also a short-lived climate forcer regulated by both China and the United States (IPCC, 2023). Understanding the NO_X budget is crucial for addressing these issues. Globally, atmospheric NO_X is mainly produced by fossil fuel combustion (Crippa et al., 2023; Huber et al., 2020; Yan et al., 2005), with smaller contributions from wildfires and lightning (Bauwens et al., 2020; Murray et al., 2012). Additionally, soil generates substantial NO_X through nitrification and denitrification processes (Bouwman et al., 2002; Cárdenas et al., 1993; Davidson, 1992; Yan et al., 2005), particularly after rainfall (Galbally and Roy, 1978; Huber et al., 2020; Yienger and Levy, 1995). On a regional scale, soil NO_X emissions maybe even exceed those from fossil fuel sources in summer (Almaraz et al., 2018; Sha et al., 2021). Model- and satellite-based studies estimate that global annual soil NO_X emissions, primarily from cultivated croplands (Almaraz et al., 2018; Huber et al., 2020; Tang et al., 2020), range from 9 to 27 Tg N, accounting for about 25% of total NO_x emissions (Oikawa et al., 2015). This wide range is due to the complex response of soil NO_X emissions to driving factors like fertilization, temperature, and soil moisture (Huber et al., 2020; Oikawa et al., 2015), making accurate estimation challenging.

Limited observations indicate that natural soil NO_x fluxes are generally below 2.50 Mg N km^{-2} yr^{-1} (Almaraz et al., 2018), while emissions from fertilized croplands are 1 to 2 orders of magnitude higher than nearby grasslands and forest soils (Almaraz et al., 2018; Guo et al., 2020). Recent studies show significant NO_x emissions from croplands post-fertilization, exceeding pre-fertilization rates by an order of magnitude (Almaraz et al., 2018; Oikawa et al., 2015). Despite these robust evidences of strong NO_X emissions from agricultural fertilization, the lack of extensive *in-situ* measurements hinders accurate estimation of these emissions and

https://doi.org/10.5194/egusphere-2025-243
Preprint. Discussion started: 6 February 2025

their environmental impacts. Additionally, the effect of agricultural fertilization on air quality has not received sufficient global attention, aside from some case studies. For example, agricultural soil emissions significantly increase atmospheric NO_X levels (Almaraz et al., 2018; Oikawa et al., 2015) and O_3 concentrations in summer in California (Oikawa et al., 2015), with monthly mean NO_2 columns rising by 53.3% and surface NO_2 and O_3 concentrations increasing by 114.0% and 23.2%, respectively (Sha et al., 2021).

China has been the world's largest consumer of N-fertilizer since 2000 (Liu et al., 2013), with annual usage peaking at approximately 31.2 Tg N in 2014 (Yu et al., 2022). About half of this fertilizer is lost to the environment (Liu et al., 2013), indicating a significant potential source for NO_x emissions from China's croplands. North China, a major grain-producing region, is primarily responsible for agricultural N-fertilizer consumption (Yu et al., 2022) and has shown substantial soil NO_x emissions (Liu et al., 2010; Tang et al., 2020; Zhang et al., 2011). The emissions significantly increase ambient NO_X levels and enhance O_3 formation in summer (Wang et al., 2022), similar to the scenario in California (Sha et al., 2021). These concerns typically focus on the warm season when higher temperatures favor NO_X emissions from soils. However, frequent agricultural activities and N-fertilizer use also occur during transitional seasons (Oikawa et al., 2015), and how periodic agricultural fertilization affects soil NO_X emission and regional air quality remains unclear.

In this study, we present an unexpected pulse of atmospheric NO_2 column in early spring during the past two decades over North China. However, this phenomenon has not been previously reported. Combining agricultural fertilization records, surface NO_2 and NH_3 observations, long-term satellite observations of NO_2 and NH_3, and a flexible scheme of soil NO_X emission, we explain successfully the underlying cause for the NO_2 column peaks using a regional atmospheric transport model online coupled with chemistry, and further assess the impacts of the pulsing NO_x emission on reginal air quality.

https://doi.org/10.5194/egusphere-2025-243
Preprint. Discussion started: 6 February 2025

2 Materials and Methods

2.1 Model and configurations

The Weather Research and Forecasting model fully coupled with atmospheric chemistry (WRF-Chem, version 3.6.1) we used is a modified model by Li et al. (2011a; 2012; 2010; 2011b) and Feng et al (2021), in which we implement the BDSNP mechanism by Hudman et al. (2012) to calculate soil NO_x and NH_3 emissions related to agricultural fertilization and the influences on regional air quality in North China. The model is configured with grid spacing of 6 km × 6 km (240 × 280 grid cells) with the center at 38°N and 116°E (Figure 1). Thirty-five vertical levels are employed in the stretched vertical grid with spacing ranging from 50 m near surface, to 500 m at 2.5 km and 1 km above 14 km. Meteorological initial and boundary conditions use the National Centers for Environmental Prediction (NCEP) FNL 1°×1° analysis data, and the chemical initial and boundary conditions are interpolated from the CAM-Chem 6-h output (Buchholz et al., 2019; Emmons et al., 2020). The non-soil emission inventory is developed by Zhang et al. (2009) and the biogenic emissions are calculated online using the Model of Emissions of Gases and Aerosol from Nature (MEGAN) model (Guenther et al., 2006). The model spin-up time is 2 days (Table 1).

https://doi.org/10.5194/egusphere-2025-243
Preprint. Discussion started: 6 February 2025

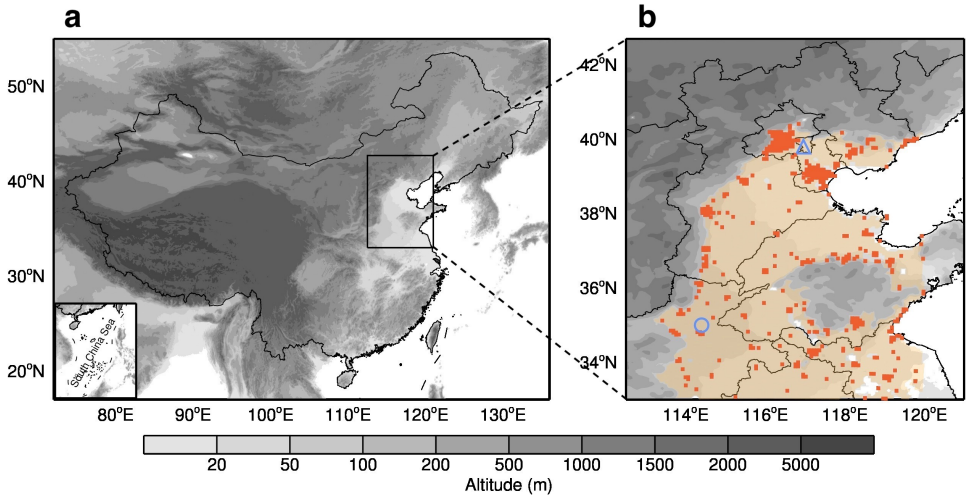

111

112 **Figure 1.** Domain overview. (**a**) Geographic location of North China, which is predominantly
113 characterized by plains at an elevation less than 100 m, and known for a major agricultural
114 zone. (**b**) Extensive cultivated croplands distribute in North China, marked by the orange
115 shadings, while urban areas are marked by red shadings. The graphic markers denote locations
116 of field observation sites, of which the blue circle represents the Fengqiu cropland ecological
117 station, Chinese Academy of Sciences, with a long-term record on agricultural fertilization,
118 and the triangle represents the rural Xianghe station with ambient NH_3 measurements.

119

120 **Table 1.** Model configuration for the simulation domain, meteorological schemes, initial and
121 boundary conditions, and emission inventories.

Item	Configuration
Period	February through April, 2020
Region	North China and surrounding areas
Domain center	116°E, 38°N
Domain size	1440 km × 1680 km
Horizontal resolution	6 km × 6 km
Vertical resolution	35 vertical levels with a stretched vertical grid with spacing ranging from 50 m near surface, to 500 m at 2.5 km and 1 km above 14 km
Microphysics scheme	WRF Single-Moment 6-class scheme [12]
Boundary layer scheme	MYJ TKE scheme [13]

https://doi.org/10.5194/egusphere-2025-243
Preprint. Discussion started: 6 February 2025

Surface layer scheme	MYJ surface scheme [13]
Land-surface scheme	Noah land surface model [14]
Longwave radiation scheme	New Goddard scheme [15]
Shortwave radiation scheme	New Goddard scheme [16]
Meteorological boundary and initial condition	NCEP FNL 1° × 1° analysis data
Chemical boundary and initial condition	CAM-Chem 6-h output [17,18]
Anthropogenic emission inventory	MEIC emission inventory [19,20]
Biogenic emission inventory	MEGAN model [21]
NOx emission from various types of soils	Soil NO_x emission mechanism [1]
Spin-up time	2 days

2.2 Soil NO_X emission scheme

We implement a soil NO_x emission scheme, the Berkeley-Dalhousie Soil NO Parameterization (BDSNP) by Hudman et al. [1], into the WRF-Chem model. The scheme comprehensively considers various factors, including available soil nitrogen content (N_{avail}) from the natural pool, fertilizer application, and nitrogen deposition, in which the soil NO_x emission (E_{soil}) is a function of N_{avail}, climate, and edaphic conditions:

$$E_{soil} = A'_{biome}(N_{avail}) \times f(T) \times g(\theta) \times P(l_{dry}) \quad (1)$$

where N_{avail} is available soil nitrogen mass, and A'_{biome} represents the biome-dependent emission factor. $f(T)$ and $g(\theta)$ are parameters regulated by soil temperature and moisture, respectively. $P(l_{dry})$ denotes the pulsed soil emission from wetting of dry soils. The product by $f(T)$ and $g(\theta)$ is calculated following:

$$f(T) \times g(\theta) = e^{0.103T} \times a\theta e^{-b\theta^2} \quad (2)$$

where T ($0 \leq T \leq 30$°C) is soil temperature and θ ($0 \leq \theta \leq 1$) is water-filled pore space, defined as the ratio of the volumetric soil moisture content to the porosity. According to the laboratory and field measurements [1], the constants a and b are determined so that $g(\theta)$ maximizes when θ = 0.2 for arid soils and θ = 0.3 elsewhere.

https://doi.org/10.5194/egusphere-2025-243
Preprint. Discussion started: 6 February 2025

The pulsing term $P(l_{dry})$, following Yan et al. [2], describes the magnitude of the peak flux relative to the pre-wetting flux, which is parameterized as:

$$P(l_{dry}) = [13.01 \ln(l_{dry}) - 53.6] \times e^{-ct} \quad (3)$$

where l_{dry} represents the length of the antecedent dry period in hours, and c (c = 0.068 h^{-1}) is a constant rate denoting the rise/fall time of the pulse. Fertilizer applications data are interpolated from the global gridded chemical fertilizer and manure application inventory at 0.5°× 0.5° [2,3]. More details of the scheme are found in related studies elsewhere [1,4].

2.3 Emission inventories

We employ two emission inventories in this study, of which the Hemispheric Transport of Air Pollution Version 3 (HTAP v3, 2005-2018) emission inventory includes soil and non-soil emissions [5], and the Multi-resolution Emission Inventory for China (MEIC v1.3, 2007-2018) has no soil emission [5]. In the HTAP inventory, the non-soil emission inventory includes energy, industry, ground transport, residential, waste, shipping and aviation sources in the HTAP inventory, with a spatial resolution of 0.1°×0.1° and a temporal resolution of one month. The monthly MEIC emission inventory with a spatial resolution of 0.25°×0.25° is incorporated in parallel with the HTAP emission inventory. Here, we focus on NO_X and NH_3 emissions from croplands with fertilization, and adopt NH_3 emission inventory by Huang et al. [6] because they explicitly distinguish NH_3 produced by agricultural fertilization from other NH_3 sources.

2.4 Air pollutant measurements

Satellite-derived NO_2 and NH_3 columns are from OMI launched by the National Aeronautics and Space Administration and the Infrared Atmospheric Sounding Interferometer (IASI) by the European Space Agency, respectively. The tropospheric column of NO_2 screened for cloud fraction less than 30% global daily composite, has a spatial resolution of 13 km × 24 km, with

https://doi.org/10.5194/egusphere-2025-243
Preprint. Discussion started: 6 February 2025

a temporal coverage of 2005-2022 (Lamsal et al., 2021), and the trajectory NH_3 from IASI is interpolated into 0.125° × 0.125° grids, with a temporal coverage of 2007-2021 (Clarisse et al., 2023). Low-quality satellite data are filtered out due to the interference of clouds. To cover all the domain (Figure 1), the data used in this study are merged into seven-day mean datasets of NO_2 and NH_3 columns.

Ambient surface NO_2, O_3, and $PM_{2.5}$ mass concentrations at 141 sites in North China are from the China National Environmental Monitoring Centre (CNEMC). These *in-situ* measurements are performed by the Thermo Scientific™ ambient particulate monitor and gas analyzers, of which NO_2 and O_3 are measured by Model 42i Chemiluminescence NO-NO_2-NO_x Analyzer, Model 49i UV Photometric Ozone Analyzer, respectively. $PM_{2.5}$ is measured by Model 5030 Synchronized Hybrid Ambient, Real-time Particulate (SHARP) Monitor, which uses proprietary digital filtering to continuously calibrate mass to obtain an accurate, precise and real-time mass concentration. Agricultural NH_3 concentration is monitored by a Picarro analyzer based on the principle of cavity ring-down spectroscopy (CRDS) at the rural Xianghe station (Figure 1).

3 Results and Discussion

3.1 Satellite-retrieved NO_2 column pulses

During the past two decades, seven-day mean tropospheric column of NO_2 measured by the Ozone Monitoring Instrument (OMI) in North China exhibits a significant temporal variation, with the magnitude varying from less than 100 μmol m^{-2} to more than 680 μmol m^{-2} (Figure 2a). The annual cycle is highly prominent and its seasonal variation is remarkable, with significantly higher levels in cold seasons than those in warm seasons. Throughout the year, the pattern of NO_2 column looks like a rhinoceros horn, which is characterized by a major peak in winter and multiple noticeable sub-peaks in other seasons. These sub-peaks often occur at

https://doi.org/10.5194/egusphere-2025-243
Preprint. Discussion started: 6 February 2025

fixed times, such as in March, June and October, of which the sub-peak is the most noticeable in March, with the highest magnitude (Figures 2a and S1). We examine the monthly variation in anthropogenic NO_X emission rates over North China in global and regional emission inventories, and find that the monthly variation is more evident in the regional emission inventory, with a significantly higher emission than that in the global emission inventory. Nevertheless, neither of them reveals any discernible sub-peaks of NO_X emission rates from fossil fuel combustion to coincide with the sub-peaks of the NO_2 column (Figure 2b).

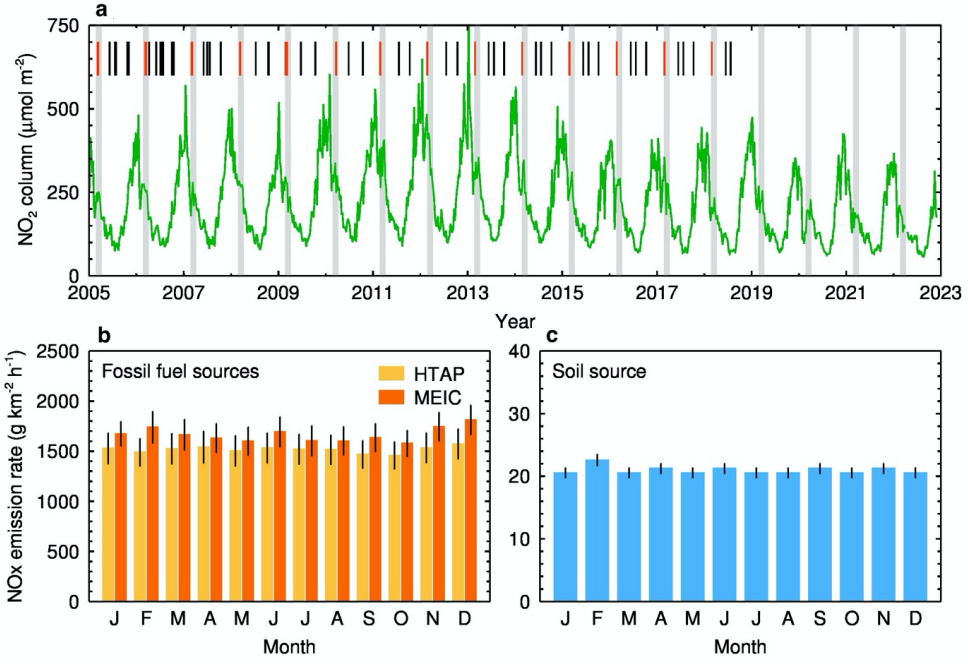

Figure 2. NO_2 column pulses in March over North China. (**a**) Long-term variation of seven-day mean tropospheric NO_2 column observed by OMI during the past two decades (2005-2022). Intersections of the gray bars and the green lines denote a sub-peak of NO_2 column occurred in each March, and the short bars represent the timing record for agricultural fertilization at Fengqiu station in North China, of which the red ones indicate the fertilization period in early spring. (**b**) Monthly mean NO_x emission rates with $\pm 1\boldsymbol{\sigma}$ standard deviation (SD) in two sets of anthropogenic emission inventories, the HTAP v3 (2005-2018, orange) and MEIC v1.3 (2008-

https://doi.org/10.5194/egusphere-2025-243
Preprint. Discussion started: 6 February 2025

2017, red). (**c**) Same as (b), but for NO_X emission rates from soils in the HTAP v3 inventory (2005-2018).

As for soil NO_X emissions, they are absent in the regional emission inventory, while in the global emission inventory, soil NO_X emissions fluctuate slightly on a monthly scale, far less than those from fossil fuel combustion, constituting less than 2% of the total (Figure 2c). Similar to NO_X emissions from fossil fuel combustion, there are no evident sub-peaks of soil NO_X emission to keep pace with the atmospheric NO_2 column. Soil NO_X emissions are even at a lower level in March, significantly less than emissions in adjacent months. Therefore, the known emission inventory fails to explain the occurrence of these sub-peaks. On the other hand, we compute a pollution accumulation index (PAI, Text S1), the product of boundary layer height and wind speed, to semi-quantitatively assess the influence of atmospheric dispersion conditions on NO_2 column. NO_2 column seems to be somewhat dependent on the PAI, yet the noticeable discrepancies between the timing of the sub-peaks and PAI are insufficient to account for the occurrence of each sub-peak (Figure S2).

3.2 Linkage between NO_2 column pulses and agricultural fertilization

What causes these regular NO_2 sub-peaks occurred over North China during the past two decades? Measurements on ammonia (NH_3) column also present similar pulses to those of NO_2 column during the same period, in spite of some differences in the long-term trend (Figures S3 and S4). These concurrent sub-peaks of NH_3 column provide favorable evidence that these NO_2 column sub-peaks are likely connected to agricultural activities because atmospheric NH_3 is largely originated from fertilizer application in agriculture (Crippa et al., 2023; Huang et al., 2012; Li et al., 2017b). Another key evidence is that the occurrence of each sub-peak of the NO_2 column is highly consistent with the record of agricultural fertilization at the Fengqiu

https://doi.org/10.5194/egusphere-2025-243
Preprint. Discussion started: 6 February 2025

cropland ecological station in North China during the past decades (Figures 1b, 2a, and S1). In North China, agricultural activities are strongly dependent on the lunar calendar. For example, agricultural fertilization is closely associated with three solar terms, i.e., Waking of Insects in March (the 3rd solar term), Grain in Beard in June (the 9th solar term) and Cold Dew in October (the 17th solar term). As already mentioned, two different satellite products reveal significant and concurrent pulses of NO_2 column and NH_3 column around these three solar terms (Figures 2a, S1, S3, and S4), indicating that they are likely originated from the same sources. During these pulses of the NO_2 column, we found that the pulse in March is more pronounced than those in June and October, because March is the season for a large-scale cultivating in North China, accompanied by more land preparation and fertilization. Therefore, we hypothesize that the NO_2 column pulse in March is possibly caused by fertilized croplands that accelerate NO_X emissions from agricultural soils. A field campaign has measured a high NO emission rate of 266.3 g km^{-2} h^{-1} in croplands after fertilization and irrigation in autumn in eastern China (2020), suggesting that agricultural fertilization is likely a significant source of atmospheric NO_X in major agricultural countries like China.

3.3 Soil NO_X emission mechanism

To examine the role of soil NO_x emissions from agricultural fertilization in the pulses of atmospheric NO_2 column, we introduce flexible soil NO_x emission and NH_3 emission modules into the WRF-Chem model, and perform two simulation experiments that include and exclude soil emissions, respectively (Table 1). Soil NO_x emission rate calculated by the model gradually increases while adding the soil NO_x emission mechanism related to agricultural fertilization. Noticeably, there is an acceleration in the release of soil NO_X, and daily mean emission rate increases from 155.6 g km^{-2} h^{-1} to 438.3 g km^{-2} h^{-1} during the simulation period (Figure 3a). In particular, the NO_X emission rate during the post-fertilization phase is significantly higher than

https://doi.org/10.5194/egusphere-2025-243
Preprint. Discussion started: 6 February 2025

254 those during other phases, consistent with the accelerated soil NO_X release observed in
255 agricultural areas in California after fertilization (Oikawa et al., 2015). On average, the
256 simulated NO_X emission rate in March is 312.9 g km^{-2} h^{-1}, between the measured 113.6 g km^{-2} h^{-1} in November in eastern China (Tang et al., 2020) and 988.2 g km^{-2} h^{-1} in September in
258 California (Oikawa et al., 2015), suggesting the rationality of the soil NO_X emission
259 mechanism in the model.

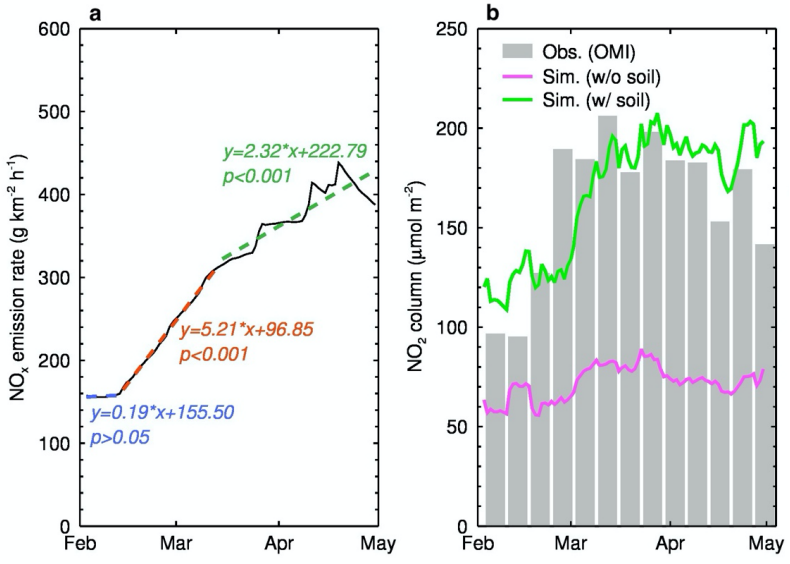

260

261 **Figure 3. NO_X emissions from agricultural fertilization and resultant NO_2 column.** (**a**)
262 Calculated NO_X emission rate from croplands with N-fertilizer application in the model. The
263 black curve represents daily variation in NO_X emission rate around the fertilization, and the
264 blue, red, and green dash lines correspond to the trends of NO_X emission rates in croplands
265 during the pre-fertilization, fertilization and post-fertilization periods, respectively. (**b**)
266 Observed and simulated NO_2 column. The gray histogram represents NO_2 column observed by
267 satellite (OMI), and the green and pink lines represent simulated NO_2 column with and without
268 soil NO_X emissions. The model well replicates the rapid increase in observed NO_2 column by
269 considering soil NO_X emissions from agricultural fertilization.

https://doi.org/10.5194/egusphere-2025-243
Preprint. Discussion started: 6 February 2025

We also evaluate the model performances against satellite-derived NO_2 column. Consequently, the modified model perfectly replicates the sudden increase in NO_2 column linked to agricultural fertilization, while the conventional WRF-Chem model fails to capture the observed NO_2 column pulse in March due to lack of the adopted soil NO_x emission mechanism (Figure 3b). For example, when soil NO_X emission caused by agricultural fertilization is considered, the simulated NO_2 column rapidly increases to the peak in March, matching well with the satellite observation. However, without the contribution of agricultural fertilization, NO_2 column seems to exhibit a weak upward trend, but not significant. Comparing these two scenarios, a substantial NO_X emission from N-fertilizer input in croplands leads to an increase in NO_2 column by 1 to 1.5 times.

We also validate the modified model performance on temporal variations in routine ground-level pollutant measurements (NO_2, O_3 and $PM_{2.5}$) associated with NO_x emissions throughout the simulation period (Figure 4). Although there are some discrepancies between the simulations and observations, e.g., overestimates occur in mid-February for NO_2 and $PM_{2.5}$ levels, the model generally reproduces hourly variations in each pollutant reasonably. The IOAs between the simulated and observed near-surface concentrations of NO_2, O_3, and $PM_{2.5}$ are 0.90, 0.91, and 0.88, respectively, and the normalized MBs (NMBs) for these pollutants are within 10%. All of these significant improvements of the modified model we used suggest that soil NO_X emission from agricultural fertilization would exert a crucial influence on regional air quality.

https://doi.org/10.5194/egusphere-2025-243
Preprint. Discussion started: 6 February 2025

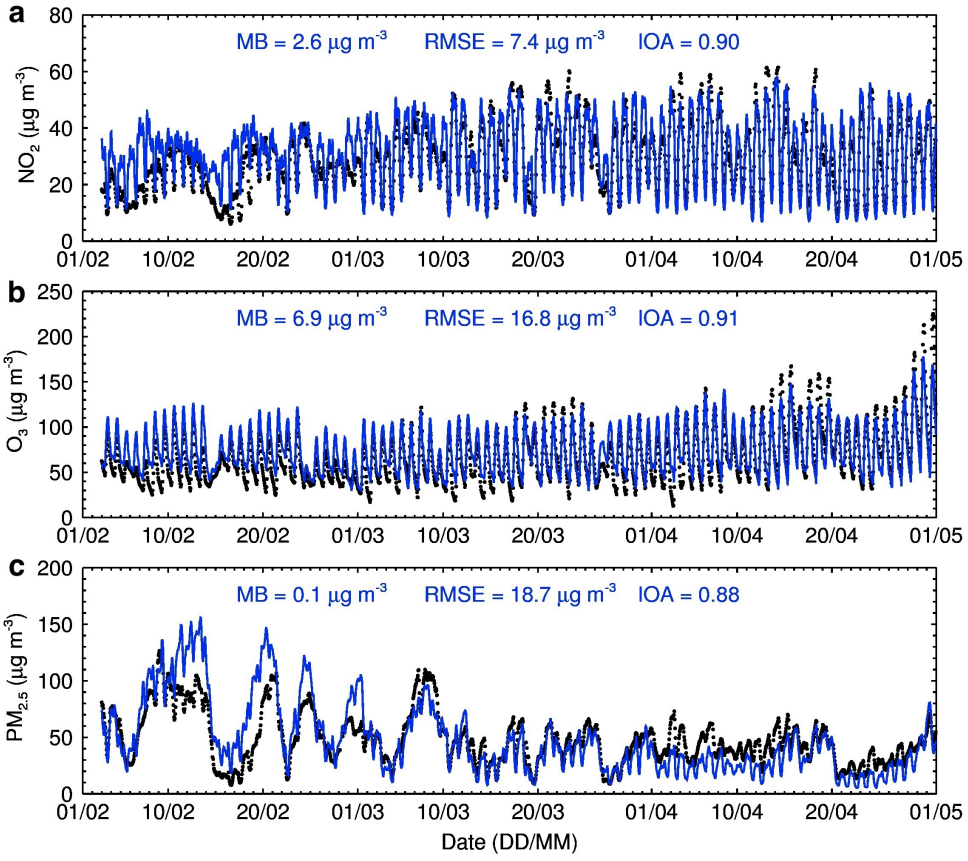

Figure 4. Simulated *vs.* measured surface pollutants. (**a** to **c**) Temporal variations in surface NO_2 (**a**), O_3 (**b**), and $PM_{2.5}$ (**c**) mass concentrations. The blue curves denote the model calculation and the black dots denote *in-situ* measurements. Model biases are shown in the central upper position of each figure.

Furthermore, we examine the ability of the model to simulate the ground-level NO_2 mass concentration and NH_3 volume concentration when soil NO_X rapidly releases after fertilization. The reason is that influences of soil emissions on atmospheric NO_2 and NH_3 concentrations are confined in the near-surface layers below 1 km, and the influences diminish rapidly as altitude increases (Figure 5). This indicates that impact of the soil emissions is primarily

https://doi.org/10.5194/egusphere-2025-243
Preprint. Discussion started: 6 February 2025

concentrated near the ground surface. With soil emissions included or not in the model, we compare the simulated NO_2 and NH_3 concentrations with near-surface observations (Figures 6a and 6b). When there are no soil NO_x emissions from agricultural fertilization, the simulated NO_2 concentration is significantly lower than the observed by 10.8 μg m^{-3}. While considering these emissions, the mean bias (MB, Text S2) between the simulation and the observation decreases to 2.1 μg m^{-3}, and the IOA also increases from 0.49 to 0.86. Similarly, the simulated NH_3 concentration is in good agreement with the observed when the soil NH_3 emission related to agricultural fertilization is involved, e.g., the MB decreases from 11.5 ppb to 2.0 ppb, and the IOA increases from 0.55 to 0.76 (Figures 6c and 6d).

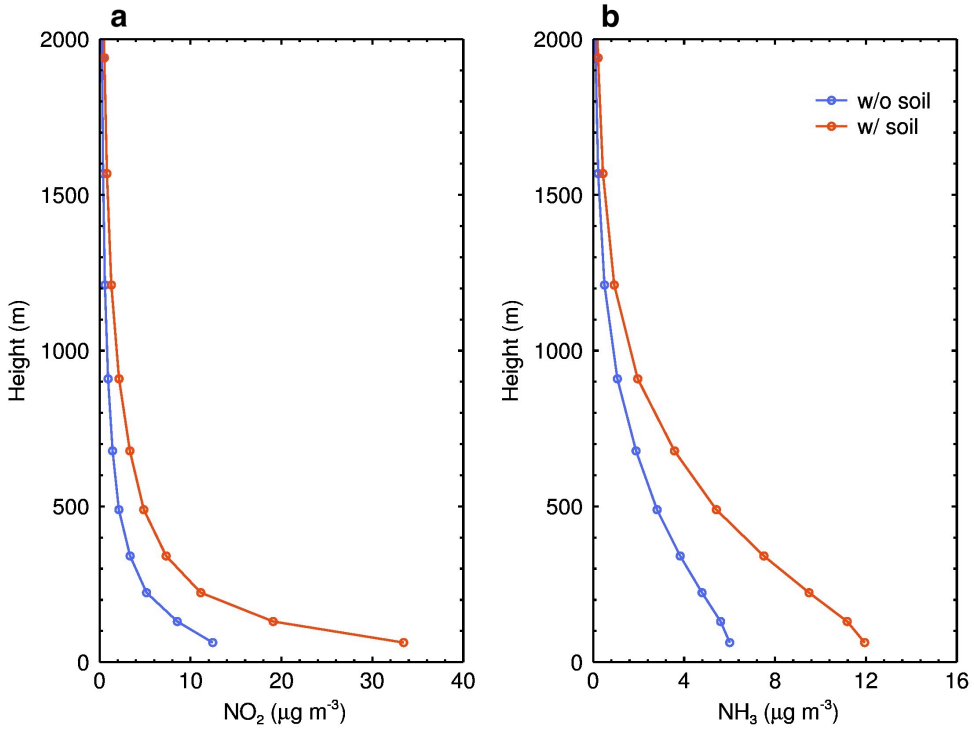

Figure 5. Vertical profiles for impacts of soil emissions on gas pollutants. (**a**) Difference in NO_2 concentration with and without the influence of soil NO_x emission from agricultural fertilization at various heights in the near-surface layers. (**b**) Similar to (**a**), but for NH_3 concentration.

https://doi.org/10.5194/egusphere-2025-243
Preprint. Discussion started: 6 February 2025

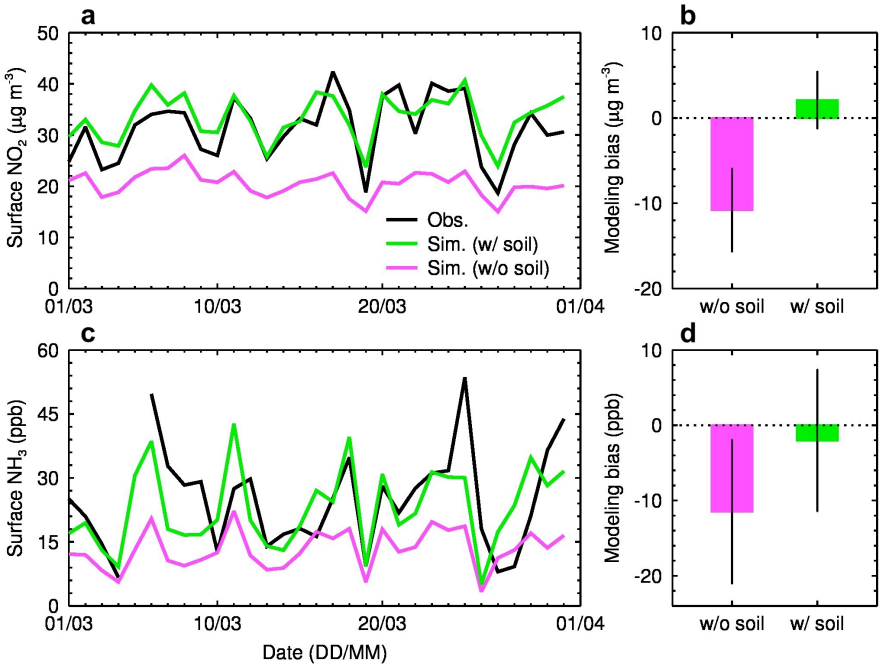

Figure 6. Contribution of soil emissions from agricultural fertilization on surface NO_2 and NH_3. (**a**-**b**) Change in surface NO_2 concentration with (green) and without (pink) soil NO_X emission from agricultural fertilization, the black line in (**a**) is for observed surface NO_2 concentration. (**c**-**d**) Same as (**a**-**b**), but for NH_3. The error bar in (**b** and **d**) denotes ±1**σ**. NO_2 observations are averaged over the 141 monitoring stations in the study area from the CNEMC network. NH_3 observations are from the rural Xianghe station (Figure S1). According to *in-situ* measurements on NO_2 and NH_3, the units for NO_2 and NH_3 concentrations are μg m^{-3} and ppb, respectively.

3.4 Significance of soil NO_X emissions from agricultural fertilization for air quality

Agricultural fertilization directly leads to substantial increases in atmospheric NO_X and NH_3 concentrations. According to the spatial correlation between land use and NO_2 concentration, NO_2 concentrations increase by more than 15 μg m^{-3} over agricultural areas, with the maximal increments occurring in the densely cultivated southern region of North China, exceeding 40

https://doi.org/10.5194/egusphere-2025-243
Preprint. Discussion started: 6 February 2025

μg m^{-3} (Figures 1b and 7a). While in urban areas, the increase in NO_2 concentration is mostly below 10 μg m^{-3}, significantly lower than those in agricultural areas. This indicates that the influence of local emissions originated from agricultural fertilization on air quality primarily concentrate in agricultural areas. Nonetheless, the influence extends to surrounding areas through atmospheric transport, leading to an inhomogeneous increase of NO_2 concentrations across North China. Spatial distribution of the increased NH_3 concentration is highly similar to that of the increased NO_2 concentration, albeit some differences exist in the southeast of North China. These differences are largely attributed to the spatial distribution of NH_3 emission rates (Huang et al., 2012).

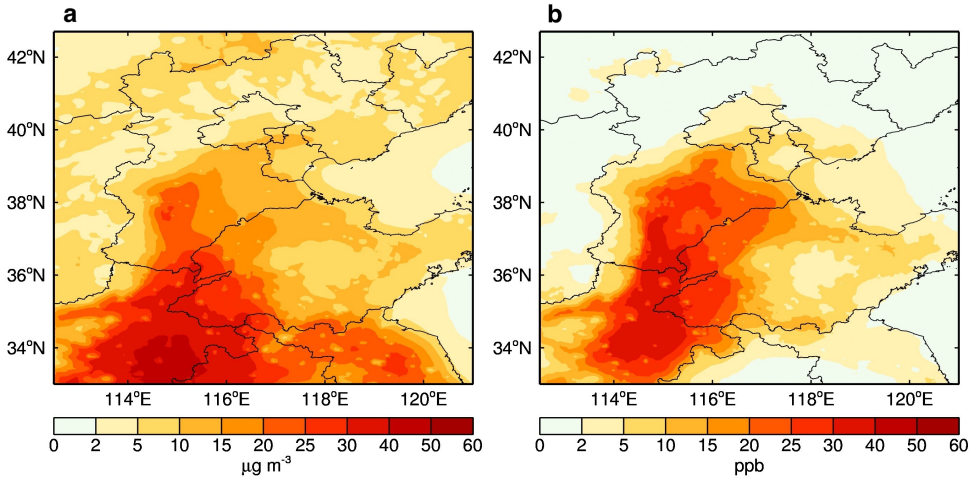

Figure 7. Direct impacts of soil emissions from agricultural fertilization on surface NO_2 and NH_3. (**a** and **b**) Spatial distributions of changes in surface NO_2 and NH_3 concentrations due to fertilization-related soil emissions in March over North China. According to *in-situ* measurements on NO_2 and NH_3, the units for NO_2 and NH_3 concentrations are μg m^{-3} and ppb, respectively.

A substantial amount of reactive nitrogen from agricultural fertilization suddenly enters the atmosphere, and further affects air quality *via* photochemical reactions and aerosol

https://doi.org/10.5194/egusphere-2025-243
Preprint. Discussion started: 6 February 2025

chemical transformations profoundly (Seinfeld and Pandis, 2006; Wu et al., 2020). Our results reveal that the NO_X emission induced by N-fertilization significantly suppresses the early-spring O_3 production in North China, which varies remarkably with the land use, approximately twice as strong in agricultural areas as in urban areas. For instance, in agricultural areas, the emission in croplands reduces nocturnal and diurnal O_3 by 30.1±6.5 μg m^{-3} (37.5±8.1%) and 15.0±3.7 μg m^{-3} (18.7±4.6%), respectively, while in urban areas, the corresponding O_3 reductions are 15.6±4.7 μg m^{-3} (15.6±4.7%) and 9.7 ±3.2 μg m^{-3} (10.6±3.4%), respectively (Figure 8). Based on the diurnal cycle of the change in O_3 concentrations ($\Delta[O_3]$), we also find that the nighttime O_3 reduction is much higher than the daytime reduction (Figure 9). The $\Delta[O_3]$ caused by agricultural fertilization is linearly and negatively correlated with the change in NO_2 concentration ($\Delta[NO_2]$) (Figures 10a-d), and the negative correlation is more pronounced at night (r = -0.997 for agricultural areas and r = -0.994 for urban areas, $p < 0.001$, Figures 10a and b). This suggests that the O_3 concentration strongly depends on the change in NO_X levels in North China during early spring. Continuous agricultural NO_X (mainly NO) emissions inhibit the O_3 formation by NO titration when the solar radiation is weak (Feng et al., 2021; Li et al., 2017a), particularly at night without sunlight. On the other hand, a negative correlation between $\Delta[NO_2]$ and the change in daytime OH radical ($\Delta[OH]_{day}$) suggests that the $\Delta[NO_2]$ also moderately regulates $\Delta[OH]_{day}$ (r = -0.50 for agricultural areas and r = -0.43 for urban areas, $p < 0.001$, Figures 10e and f) through decreasing O_3 levels and reactions of NO_2 with OH radical. Both OH radical and O_3 are critical oxidants in the atmosphere, and the decrease by the excessive NO_X emission from agricultural fertilization weakens atmospheric oxidizing capacity (AOC) (Feng et al., 2021). The decreased AOC can further slow down the oxidation processes in homogeneous and heterogeneous reactions, unfavorable for the formation of secondary aerosols.

https://doi.org/10.5194/egusphere-2025-243
Preprint. Discussion started: 6 February 2025

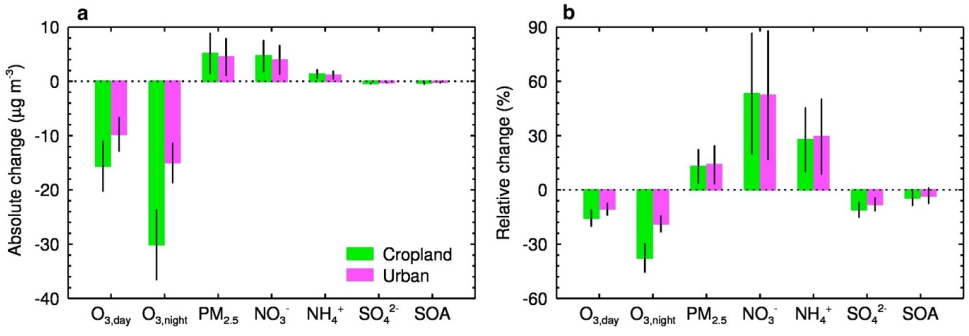

Figure 8. Complex impacts of agricultural fertilization on O_3 and $PM_{2.5}$. (**a**) Changes in mass concentrations of O_3, $PM_{2.5}$ and aerosol constituents, i.e., nitrate, ammonium, sulfate and secondary organics due to soil NO_X emission from agricultural fertilization in agricultural (green) and urban (pink) areas. The error bar denotes ±1**σ**. (**b**) Same as (**a**), but for percentage changes in O_3, $PM_{2.5}$ and aerosol constituents.

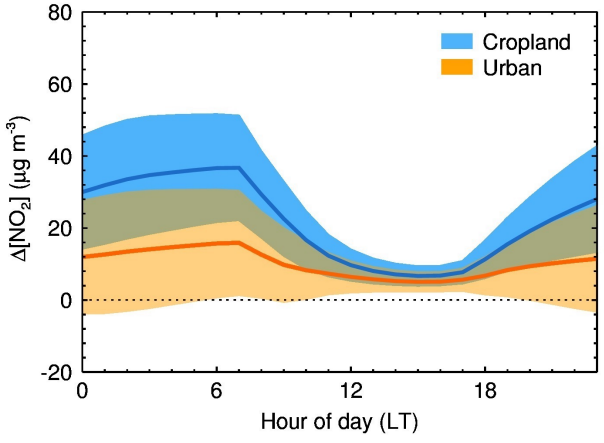

Figure 9. Secondary impact of soil NO_X emissions from agricultural fertilization on surface O_3. Diurnal cycles of changes in surface O_3 concentrations due to fertilization-related soil emissions over croplands and urban areas in North China. The blue and orange shadings show ±1**σ** of the data.

https://doi.org/10.5194/egusphere-2025-243
Preprint. Discussion started: 6 February 2025

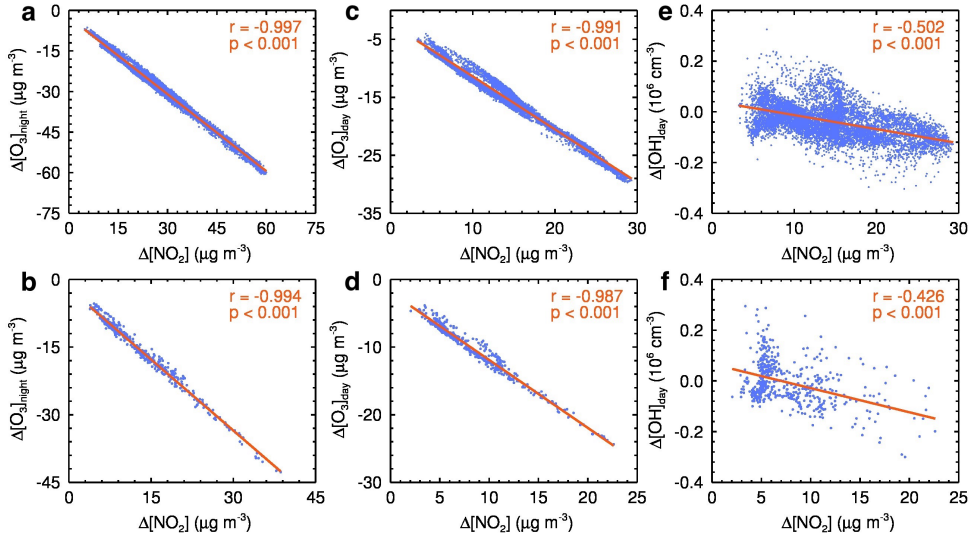

385

386 **Figure 10.** Changes in surface NO_2 and related photochemical products. (**a** to **f**) Correlation
387 between $\Delta[NO_2]$ and $\Delta[O_3]$ or $\Delta[OH]$. (**a** to **d**) Change in O_3 concentration is strongly
388 dependent on change in NO_2 concentration due to agricultural fertilization in both agricultural
389 (**a** and **c**) and urban (**b** and **d**) areas, and the dependence is more pronounced at night, i.e.,
390 correlation coefficient r = -0.997 (r = -0.994) at night and r = -0.991 (r = -0.987) at daytime in
391 agricultural (urban) areas. (**e** and **f**) Change in daytime OH radical is also significantly
392 influenced by change in NO_2 concentration in both agricultural (**e**) and urban (**f**) areas.

393

394 Interestingly, these findings are inconsistent with previous studies revealing that
395 agricultural NO_X emissions enhance the O_3 formation in summer over North China (Wang et
396 al., 2023) and in the Imperial Valley, California (Oikawa et al., 2015). This is largely attributed
397 to the sensitivity of O_3 to its precursors under different conditions of solar radiation. During
398 early spring, the insolation is relatively weak, unfavorable for the O_3 photochemical production
399 in North China. As a result, a large amount of agricultural NO_X (mainly NO) emission even
400 causes a NO titration effect during daytime, decreasing O_3 concentrations. In contrast, the
401 intensified solar radiation in summer significantly facilitates the O_3 photochemical production,

https://doi.org/10.5194/egusphere-2025-243
Preprint. Discussion started: 6 February 2025

shifting the O_3 chemistry from VOCs-sensitive to NOx-sensitive. In this scenario, the O_3 production is primarily controlled by NO_X emissions, meaning that the O_3 concentration increases with rising NO_X levels. This seasonal difference in O_3 sensitivity to its precursors highlights a seasonally dependent response of O_3 production to agricultural fertilization.

We also quantify the impact of agricultural fertilization on $PM_{2.5}$ concentrations. The North China is characterized by an excess of NH_3, in which nitrate formation is highly sensitive to NO_2 concentration and AOC due to NO_2 oxidation to NO_3^- *via* gas-phase and heterogeneous reactions (Feng et al., 2018; Fu et al., 2020; Liu et al., 2019; Wen et al., 2018). As atmospheric NO_2 and NH_3 concentrations rapidly increase due to emissions from fertilized croplands, nitrate aerosol in agricultural (urban) areas rises by 4.7 (4.0) μg m^{-3}, corresponding to the increased percentage of 53.2% (52.3%), while ammonium aerosol rises by 1.3 (1.1) μg m^{-3} in agricultural (urban) areas, with an increased percentage of 27.7% (29.4%) (Figure 8). However, sulfate aerosol shows a slight decrease both in agricultural and urban areas (Figure 8a). The reason is that an extra NO_X emission from agricultural fertilization enhances nitrate formation but lowers AOC, which hinders sulfate formation. Similar to sulfate aerosol, secondary organic aerosol (SOA) also has a slight reduction (Figure 8a). The formation of SOA greatly depends on the AOC level, so decreased AOC due to NO_x emission from agricultural fertilization does not favor the conversion of organic precursors, such as VOCs and semi-volatile primary organic aerosols, into SOA.

In general, due to agricultural fertilization, $PM_{2.5}$ concentration increases by 5.1 (4.5) μg m^{-3} (Figure 8a), corresponding to a percentage change of 12.9% (13.9%) over agricultural (urban) areas in North China (Figure 8b). There is no significant difference in $PM_{2.5}$ increments between agricultural and urban areas. Nitrate aerosol is primarily responsible for the increased $PM_{2.5}$, accounting for 92.2% and 88.9% in these two types of regions, respectively. Our results also indicate that changes in $PM_{2.5}$ and nitrate in urban areas are more sensitive to the change

https://doi.org/10.5194/egusphere-2025-243
Preprint. Discussion started: 6 February 2025

in NO_2 concentration. For instance, the ratios of nitrate change to NO_2 change ($\Delta[NO_3^-]/\Delta[NO_2]$ = 0.20) and $PM_{2.5}$ change to NO_2 change ($\Delta[PM_{2.5}]/\Delta[NO_2]$ = 0.24) in urban areas are both higher than those in agricultural areas ($\Delta[NO_3^-]/\Delta[NO_2]$ = 0.13 and $\Delta[PM_{2.5}]/\Delta[NO_2]$ = 0.15, Figures 11a and b), indicating that the conversion of NO_2 to nitrate aerosol is more efficient in urban areas. Consequently, the increased percentages of $PM_{2.5}$ and ammonium aerosol in urban areas are higher than those in agricultural areas (Figure 8b). Additionally, the ongoing stringent control measures on emission sources significantly reduce anthropogenic emissions in urban areas, thus the impact of agricultural fertilization on urban air quality is becoming more pronounced. As global warming is ongoing, routine events like agricultural fertilization will continue to have amplified impacts on air quality with the joint help of atmospheric dispersion/transport and chemical transformation processes. These impacts are not confined in agricultural areas alone, but extend to surrounding cities.

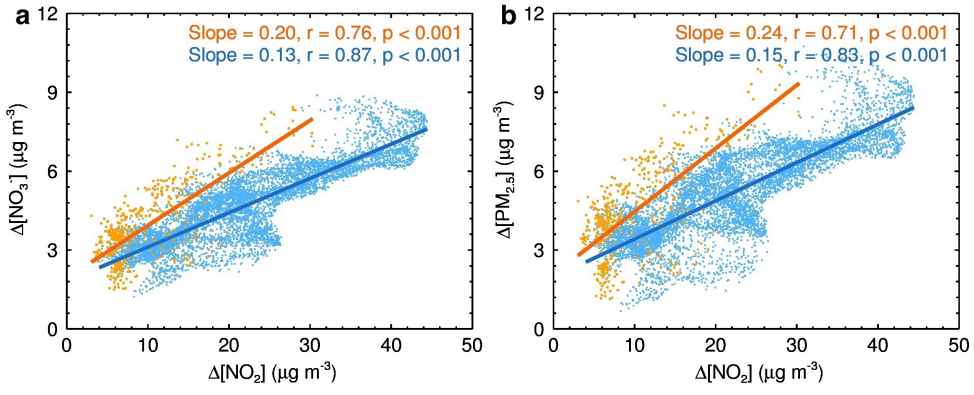

Figure 11. Changes in surface NO_2 and related aerosol-chemistry products. (**a**) Comparison of NO_2 conversion to nitrate aerosol (NO_3^-) formation between agricultural and urban areas, i.e., $\Delta[NO_3^-]/\Delta[NO_2]$ = 0.20 in urban areas and $\Delta[NO_3^-]/\Delta[NO_2]$ = 0.13 in agricultural areas, indicates that change in nitrate in urban areas are more sensitive to the change in NO_2 concentration and NO_2 conversion to NO_3^- is more efficient. (**b**) NO_2 conversion to $PM_{2.5}$ formation is similar to (**a**), because nitrate aerosol is the most affected among the various

https://doi.org/10.5194/egusphere-2025-243
Preprint. Discussion started: 6 February 2025

aerosol constituents. The blue and orange colors correspond to the agricultural and urban areas, respectively.

4 Summary and Conclusions

Impact of soil NO_X emissions from agricultural fertilization on the atmospheric environment remains unclear worldwide. In particular, this issue has not yet received enough attention in China, where substantial N-fertilizers are year by year consumed due to extensive agricultural cultivation areas. Our results indicate that agricultural fertilization is highly responsible for the periodic pulse of the atmospheric NO_2 column in North China over the past two decades. A long-term fertilization record and model results both provide sufficient evidence to illustrate their cause-to-effect relationship. For example, the fertilization timing is found to match well with the occurrence of satellite-derived NO_2 column pulse in the region. Moreover, the model reasonably captures the regular sub-peak of the NO_2 column in March by introducing an independent module that specifically describes soil NO_X emissions from agricultural fertilization.

These additional NO_X emissions released by croplands directly leads to an elevated level of surface NO_X concentrations. Consequently, the increased atmospheric NO_X concentration significantly inhibits O_3 production in early spring, distinct from the impacts in summer (Sha et al., 2021; Wang et al., 2022), but enhances nitrate formation. For example, soil emissions linked to agricultural fertilization dramatically reduce nighttime O_3 concentrations by 30.1 μg m^{-3} and 15.0 μg m^{-3} in croplands and urban areas, respectively. During daytime, the decreased O_3 concentration is 15.6 μg m^{-3} and 9.7 μg m^{-3}, respectively. In contrast, soil emissions elevate ambient $PM_{2.5}$ concentrations by more than 4.5 μg m^{-3}, accounting for 12% of the $PM_{2.5}$ mass over North China. The opposite effects are challengeable for China to improve air quality, because China is the world's largest consumer of food, of which food production strongly

https://doi.org/10.5194/egusphere-2025-243
Preprint. Discussion started: 6 February 2025

depends on N-fertilizers input. As the emission from fossil fuel combustion has been gradually decreasing, emissions from agricultural fertilization are with increasing implications for air quality. In the other hand, NO_X emission from soils is highly temperature-dependent (Hudman et al., 2012; Yienger and Levy, 1995), which is facilitated by higher temperature. Therefore, future global warming likely poses a challenge of enhanced NO_X emission from croplands, which complicates regional air pollution. We thus highlight that reducing NO_X emissions from agricultural fertilization is of great importance to air quality improvement. Policymakers should manage to reduce emissions from N-fertilizers application, for example, improving N-fertilizers efficiency and developing alternative fertilizers friendly to the environment are highly necessary. These measures will greatly minimize the adverse effects of agricultural fertilization on air quality, human health, and the ecological environment.

Code/Data availability

The OMI satellite data are from the NASA Goddard Space Flight Center, Goddard Earth Sciences Data and Information Services Center (GES DISC) (https://disc.gsfc.nasa.gov/datasets/OMI_MINDS_NO2d_1.1/summary) and the IASI satellite observations are from the IASI Portal (https://iasi.aeris-data.fr/nh3_iasi_a_arch). The real-time hourly air pollutant measurements including NO_2, O_3, and $PM_{2.5}$ are released by Ministry of Ecology and Environment, China and can be accessed on the website http://beijingair.sinaapp.com. The MEIC Group and the EDGAR Team for the MEIC and HATP emission inventories which are available at http://www.meicmodel.org and https://edgar.jrc.ec.europa.eu/dataset_htap_v3, respectively.

Author contribution

https://doi.org/10.5194/egusphere-2025-243
Preprint. Discussion started: 6 February 2025

TF and GL conceptualized the ideas, verified the conclusions, and revised the paper. TF conducted research, designed the experiments, carried out the methodology, performed the simulation, processed the data, prepared the data visualization, and prepared the paper, with contributions from all authors. SZ and NB provided the treatment of meteorological data, analyzed the study data, validated the model performance, and reviewed the paper. XL, YP, YS, and RW provided the observation data and emission inventories, and reviewed the paper. XT and LM provided critical reviews in the pre-publication stage.

Competing interests

The authors declare no conflicts of interest relevant to this study.

Acknowledgments

This work was supported by the National Natural Science Foundation of China (Grants 42371080 and 42371093), the Natural Science Foundation of Shaanxi Province (Grant 2017JM4023), and the Science and Technology Innovation 2025 Major Project of Ningbo City (Grants 2022Z032, 2022Z189, and 2023Z139). This study was also sponsored by K. C. Wong Magna Fund in Ningbo University.

References

Almaraz, M., Bai, E., Wang, C., Trousdell, J., Conley, S., Faloona, I. and Houlton, B. Z.: Agriculture is a major source of NOx pollution in California, Sci Adv, 4(1), eaao3477, doi:10.1126/sciadv.aao3477, 2018.

Bauwens, M., Compernolle, S., Stavrakou, T., Müller, J. F., van Gent, J., Eskes, H., Levelt, P. F., van der A, R., Veefkind, J. P., Vlietinck, J., Yu, H. and Zehner, C.: Impact of Coronavirus Outbreak on NO_2 Pollution Assessed Using TROPOMI and OMI Observations, Geophys. Res. Lett., 47(1), e87978, doi:10.1029/2020GL087978, 2020.

Bouwman, A. F., Boumans, L. J. M. and Batjes, N. H.: Modeling global annual N_2O and NO emissions from fertilized fields, Global Biogeochem. Cycles, 16(4), 1080–28–9,

https://doi.org/10.5194/egusphere-2025-243
Preprint. Discussion started: 6 February 2025

doi:10.1029/2001GB001812, 2002.

Buchholz, R. R., Emmons, L. K., Tilmes, S. and The CESM Development Team: CESM2.1/CAM-chem Instantaneous Output for Boundary Conditions, UCARNCAR - Atmospheric Chemistry Observations and Modeling Laboratory, doi:10.5065/NMP7-EP60, 2019.

Cárdenas, L., Rondón, A., Johansson, C. and Sanhueza, E.: Effects of soil moisture, temperature, and inorganic nitrogen on nitric oxide emissions from acidic tropical savannah soils, J Geophys Res, 98(D8), 14783–14790, doi:10.1029/93JD01020, 1993.

Clarisse, L., Franco, B., Van Damme, M., Di Gioacchino, T., Hadji-Lazaro, J., Whitburn, S., Noppen, L., Hurtmans, D., Clerbaux, C. and Coheur, P.: The IASI NH_3 version 4 product: averaging kernels and improved consistency, Atmos. Meas. Tech., 16(21), 5009–5028, doi:10.5194/amt-16-5009-2023, 2023.

Crippa, M., Guizzardi, D., Butler, T., Keating, T., Wu, R., Kaminski, J., Kuenen, J., Kurokawa, J., Chatani, S., Morikawa, T., Pouliot, G., Racine, J., Moran, M. D., Klimont, Z., Manseau, P. M., Mashayekhi, R., Henderson, B. H., Smith, S. J., Suchyta, H., Muntean, M., Solazzo, E., Banja, M., Schaaf, E., Pagani, F., Woo, J.-H., Kim, J., Monforti-Ferrario, F., Pisoni, E., Zhang, J., Niemi, D., Sassi, M., Ansari, T. and Foley, K.: The HTAP_v3 emission mosaic: merging regional and global monthly emissions (2000–2018) to support air quality modelling and policies, Earth System Science Data, 15(6), 2667–2694, doi:10.5194/essd-15-2667-2023, 2023.

Davidson, E. A.: Sources of nitric oxide and nitrous oxide following wetting of dry soil, Soil Science Society of America Journal, 56(1), 95–102, doi:10.2136/sssaj1992.03615995005600010015x, 1992.

Emmons, L. K., Schwantes, R. H., Orlando, J. J., Tyndall, G., Kinnison, D., Lamarque, J.-F., Marsh, D., Mills, M. J., Tilmes, S., Bardeen, C., Buchholz, R. R., Conley, A., Gettelman, A., Garcia, R., Simpson, I., Blake, D. R., Meinardi, S. and Pétron, G.: The Chemistry Mechanism in the Community Earth System Model Version 2 (CESM2), J. Adv. Model. Earth Syst., 12(4), e2019MS001882, doi:10.1029/2019MS001882, 2020.

Feng, T., Bei, N., Zhao, S., Wu, J., Li, X., Zhang, T., Cao, J., Zhou, W. and Li, G.: Wintertime nitrate formation during haze days in the Guanzhong basin, China: A case study, Environ. Pollut., 243, 1057–1067, doi:10.1016/j.envpol.2018.09.069, 2018.

Feng, T., Zhao, S., Hu, B., Bei, N., Zhang, X., Wu, J., Li, X., Liu, L., Wang, R., Tie, X. and Li, G.: Assessment of Atmospheric Oxidizing Capacity Over the Beijing-Tianjin-Hebei (BTH) Area, China, J. Geophys. Res. Atmos., 126(7), e2020JD033834, doi:10.1029/2020JD033834, 2021.

Fu, X., Wang, T., Gao, J., Wang, P., Liu, Y., Wang, S., Zhao, B. and Xue, L.: Persistent

559 Heavy Winter Nitrate Pollution Driven by Increased Photochemical Oxidants in Northern
560 China, Environ. Sci. Technol., 54(7), 3881–3889, doi:10.1021/acs.est.9b07248, 2020.

561 Galbally, I. E. and Roy, C. R.: Loss of fixed nitrogen from soils by nitric oxide exhalation,
562 Nature, 275(5), 734–735, doi:10.1038/275734a0, 1978.

563 Guenther, A., Karl, T., Harley, P., Wiedinmyer, C., Palmer, P. I. and Geron, C.: Estimates of
564 global terrestrial isoprene emissions using MEGAN (Model of Emissions of Gases and
565 Aerosols from Nature), Atmos. Chem. Phys., 6(11), 3181–3210, doi:10.5194/acp-6-3181-
566 2006, 2006.

567 Guo, L., Chen, J., Luo, D., Liu, S., Lee, H. J., Motallebi, N., Fong, A., Deng, J., Rasool, Q.
568 Z., Avise, J. C., Kuwayama, T., Croes, B. E. and FitzGibbon, M.: Assessment of Nitrogen
569 Oxide Emissions and San Joaquin Valley $PM_{2.5}$ Impacts From Soils in California, J.
570 Geophys. Res. Atmos., 125(24), e2020JD033304, doi:10.1029/2020JD033304, 2020.

571 Huang, X., Song, Y., Li, M., Li, J., Huo, Q., Cai, X., Zhu, T., Hu, M. and Zhang, H.: A high-
572 resolution ammonia emission inventory in China, Global Biogeochem. Cycles, 26(1),
573 GB1030, doi:10.1029/2011GB004161, 2012.

574 Huber, D. E., Steiner, A. L. and Kort, E. A.: Daily Cropland Soil NOx Emissions Identified
575 by TROPOMI and SMAP, Geophys. Res. Lett., 47(2), e89949, doi:10.1029/2020GL089949,
576 2020.

577 Hudman, R. C., Moore, N. E., Mebust, A. K., Martin, R. V., Russell, A. R., Valin, L. C. and
578 Cohen, R. C.: Steps towards a mechanistic model of global soil nitric oxide emissions:
579 implementation and space based-constraints, Atmos. Chem. Phys., 12(1), 7779–7795,
580 doi:10.5194/acp-12-7779-2012, 2012.

581 IPCC: Short-lived Climate Forcers, in Climate Change 2021 – The Physical Science Basis:
582 Working Group I Contribution to the Sixth Assessment Report of the Intergovernmental
583 Panel on Climate Change, pp. 817–922, Cambridge University Press, Cambridge. 2023.

584 Lamsal, L. N., Krotkov, N. A., Vasilkov, A., Marchenko, S., Qin, W., Yang, E.-S., Fasnacht,
585 Z., Joiner, J., Choi, S., Haffner, D., Swartz, W. H., Fisher, B. and Bucsela, E.: Ozone
586 Monitoring Instrument (OMI) Aura nitrogen dioxide standard product version 4.0 with
587 improved surface and cloud treatments, Atmos. Meas. Tech., 14(1), 455–479,
588 doi:10.5194/amt-14-455-2021, 2021.

589 Li, G., Bei, N., Cao, J., Wu, J., Long, X., Feng, T., Dai, W., Liu, S., Zhang, Q. and Tie, X.:
590 Widespread and persistent ozone pollution in eastern China during the non-winter season of
591 2015: observations and source attributions, Atmos. Chem. Phys., 17(4), 2759–2774,
592 doi:10.5194/acp-17-2759-2017, 2017a.

593 Li, G., Bei, N., Tie, X. and Molina, L. T.: Aerosol effects on the photochemistry in Mexico

https://doi.org/10.5194/egusphere-2025-243
Preprint. Discussion started: 6 February 2025

City during MCMA-2006/MILAGRO campaign, Atmos. Chem. Phys., 11(11), 5169–5182, doi:10.5194/acp-11-5169-2011, 2011a.

Li, G., Lei, W., Bei, N. and Molina, L. T.: Contribution of garbage burning to chloride and $PM_{2.5}$ in Mexico City, Atmos. Chem. Phys., 12(18), 8751–8761, doi:10.5194/acp-12-8751-2012, 2012.

Li, G., Lei, W., Zavala, M., Volkamer, R., Dusanter, S., Stevens, P. and Molina, L. T.: Impacts of HONO sources on the photochemistry in Mexico City during the MCMA-2006/MILAGO Campaign, Atmos. Chem. Phys., 10(14), 6551–6567, doi:10.5194/acp-10-6551-2010, 2010.

Li, G., Zavala, M., Lei, W., Tsimpidi, A. P., Karydis, V. A., Pandis, S. N., Canagaratna, M. R. and Molina, L. T.: Simulations of organic aerosol concentrations in Mexico City using the WRF-CHEM model during the MCMA-2006/MILAGRO campaign, Atmos. Chem. Phys., 11(8), 3789–3809, doi:10.5194/acp-11-3789-2011, 2011b.

Li, M., Liu, H., Geng, G., Hong, C., Liu, F., Song, Y., Tong, D., Zheng, B., Cui, H., Man, H., Zhang, Q. and He, K.: Anthropogenic emission inventories in China: A review, National Science Review, 4(6), 834–866, doi:10.1093/nsr/nwx150, 2017b.

Liu, C., Zheng, X., Zhou, Z., Han, S., Wang, Y., Wang, K., Liang, W., Li, M., Chen, D. and Yang, Z.: Nitrous oxide and nitric oxide emissions from an irrigated cotton field in Northern China, Plant Soil, 332(1), 123–134, doi:10.1007/s11104-009-0278-5, 2010.

Liu, L., Wu, J., Liu, S., Li, X., Zhou, J., Feng, T., Qian, Y., Cao, J., Tie, X. and Li, G.: Effects of organic coating on the nitrate formation by suppressing the N_2O_5 heterogeneous hydrolysis: a case study during wintertime in Beijing–Tianjin–Hebei (BTH), Atmos. Chem. Phys., 19(12), 8189–8207, doi:10.5194/acp-19-8189-2019, 2019.

Liu, X., Zhang, Y., Han, W., Tang, A., Shen, J., Cui, Z., Vitousek, P., Erisman, J. W., Goulding, K., Christie, P., Fangmeier, A. and Zhang, F.: Enhanced nitrogen deposition over China, Nature, 494(7438), 459–462, doi:10.1038/nature11917, 2013.

Murray, L. T., Jacob, D. J., Logan, J. A., Hudman, R. C. and Koshak, W. J.: Optimized regional and interannual variability of lightning in a global chemical transport model constrained by LIS/OTD satellite data, J. Geophys. Res. Atmos., 117(D), D20307, doi:10.1029/2012JD017934, 2012.

Oikawa, P. Y., Ge, C., Wang, J., Eberwein, J. R., Liang, L. L., Allsman, L. A., Grantz, D. A. and Jenerette, G. D.: Unusually high soil nitrogen oxide emissions influence air quality in a high-temperature agricultural region, Nat. Commun., 6(1), 8753–10, doi:10.1038/ncomms9753, 2015.

Seinfeld, J. H. and Pandis, S. N.: Atmospheric Chemistry and Physics - From Air Pollution to

https://doi.org/10.5194/egusphere-2025-243
Preprint. Discussion started: 6 February 2025

Climate Change, 2nd ed., John Wiley & Sons, New Jersey. 2006.

Sha, T., Ma, X., Zhang, H., Janechek, N., Wang, Y., Wang, Y., Castro García, L., Jenerette, G. D. and Wang, J.: Impacts of Soil NOx Emission on O_3 Air Quality in Rural California, Environ. Sci. Technol., 55(10), 7113–7122, doi:10.1021/acs.est.0c06834, 2021.

Tang, K., Qin, M., Fang, W., Duan, J., Meng, F., Ye, K., Zhang, H., Xie, P., Liu, J., Liu, W., Feng, Y., Huang, Y. and Ni, T.: An automated dynamic chamber system for exchange flux measurement of reactive nitrogen oxides (HONO and NOx) in farmland ecosystems of the Huaihe River Basin, China, Sci. Total Environ., 745(C), 140867, doi:10.1016/j.scitotenv.2020.140867, 2020.

Wang, R., Bei, N., Pan, Y., Wu, J., Liu, S., Li, X., Yu, J., Jiang, Q., Tie, X. and Li, G.: Urgency of controlling agricultural nitrogen sources to alleviate summertime air pollution in the North China Plain, Chemosphere, 311(P2), 137124, doi:10.1016/j.chemosphere.2022.137124, 2023.

Wang, R., Bei, N., Wu, J., Li, X., Liu, S., Yu, J., Jiang, Q., Tie, X. and Li, G.: Cropland nitrogen dioxide emissions and effects on the ozone pollution in the North China plain, Environ. Pollut., 294, 118617, doi:10.1016/j.envpol.2021.118617, 2022.

Wen, L., Xue, L., Wang, X., Xu, C., Chen, T., Yang, L., Wang, T., Zhang, Q. and Wang, W.: Summertime fine particulate nitrate pollution in the North China Plain: increasing trends, formation mechanisms and implications for control policy, Atmos. Chem. Phys., 18(15), 11261–11275, doi:10.5194/acp-18-11261-2018, 2018.

Wu, J., Bei, N., Hu, B., Liu, S., Wang, Y., Shen, Z., Li, X., Liu, L., Wang, R., Liu, Z., Cao, J., Tie, X., Molina, L. T. and Li, G.: Aerosol–photolysis interaction reduces particulate matter during wintertime haze events, Proc. Natl. Acad. Sci. U.S.A., 117(18), 9755–9761, doi:10.1073/pnas.1916775117, 2020.

Yan, X., Ohara, T. and Akimoto, H.: Statistical modeling of global soil NOx emissions, Global Biogeochem. Cycles, 19(3), GB3019, doi:10.1029/2004GB002276, 2005.

Yienger, J. J. and Levy, H.: Empirical model of global soil-biogenic NOx emissions, J. Geophys. Res. Atmos., 100(D), 11447–11464, doi:10.1029/95JD00370, 1995.

Yu, Z., Liu, J. and Kattel, G.: Historical nitrogen fertilizer use in China from 1952 to 2018, Earth System Science Data, 14(11), 5179–5194, doi:10.5194/essd-14-5179-2022, 2022.

Zhang, Q., Streets, D. G. and Carmichael, G. R.: Asian emissions in 2006 for the NASA INTEX-B mission, Atmos. Chem. Phys., 9(14), 5131–5153, doi:10.5194/acp-9-5131-2009, 2009.

Zhang, R., Wang, G., Guo, S., Zamora, M. L., Ying, Q., Lin, Y., Wang, W., Hu, M. and

https://doi.org/10.5194/egusphere-2025-243
Preprint. Discussion started: 6 February 2025

663 Wang, Y.: Formation of urban fine particulate matter, Chem. Rev., 115(10), 3803–3855,
664 doi:10.1021/acs.chemrev.5b00067, 2015.

665 Zhang, Y., Liu, J., Mu, Y., Pei, S., Lun, X. and Chai, F.: Emissions of nitrous oxide, nitrogen
666 oxides and ammonia from a maize field in the North China Plain, Atmos. Environ., 45(17),
667 2956–2961, doi:10.1016/j.atmosenv.2010.10.052, 2011.

668